

Transiting Planets with LSST I: Potential for LSST Exoplanet Detection

Michael B. Lund¹

Joshua Pepper²¹

Keivan G. Stassun¹³

ABSTRACT

The Large Synoptic Survey Telescope (LSST) has been designed in order to satisfy several different scientific objectives that can be addressed by a ten-year synoptic sky survey. However, LSST will also provide a large amount of data that can then be exploited for additional science beyond its primary goals. We demonstrate the potential of using LSST data to search for transiting exoplanets, and in particular to find planets orbiting host stars that are members of stellar populations that have been less thoroughly probed by current exoplanet surveys. We find that existing algorithms can detect in simulated LSST light curves the transits of Hot Jupiters around solar-type stars, Hot Neptunes around K dwarfs, and planets orbiting stars in the Large Magellanic Cloud. We also show that LSST would have the sensitivity to potentially detect Super-Earths orbiting red dwarfs, including those in habitable zone orbits, if they are present in some fields that LSST will observe. From these results, we make the case that LSST has the ability to provide a valuable contribution to exoplanet science.

Subject headings: planetary systems — planets and satellites: detection — surveys

1. Introduction

The search for transiting exoplanets has produced a known exoplanet population with measurable masses and radii, largely due to the contributions of the *Kepler* mission (Batalha et al. 2013). However, this largely represents planets with host stars that are predominantly F, G, and K dwarfs in the solar neighborhood. The same is true for most planets discovered through ground-based transit surveys, such as HATnet (Bakos & Hartman 2011), TrES (O’Donovan & Charbonneau 2007), SuperWASP (Doyle et al. 2012), XO (Poleski et al. 2010), KELT (Pepper et al. 2007), and RV surveys, such as the Anglo-Australian Planet Search (Tinney et al. 2001), HARPS (Zechmeister et al. 2013), California and Carnegie Planet Search (Patel et al. 2007), and the Lick Planet Search (Fischer et al. 2014). Due to a variety of observational and selection

¹Department of Physics and Astronomy, Vanderbilt University, Nashville, TN 37235, USA; michael.b.lund@vanderbilt.edu

²Department of Physics, Lehigh University, Bethlehem, PA 18015, USA

³Department of Physics, Fisk University, Nashville, TN 37208, USA

biases, populations other than nearby mid-type dwarfs have not been examined as thoroughly, including late-type stars, evolved stars, stars outside the solar neighborhood, young stars, stellar remnants, and others. As a consequence, while *Kepler* has probed for the presence of earth-sized planets and produced a sufficient sample of planets to characterize frequency as a function of mass, radius, and period (Howard et al. 2012; Petigura et al. 2013; Youdin 2011), the current exoplanet sample does not include stellar hosts that are fully representative of all possibilities.

In this paper, we introduce an analytic- and simulation-based effort to explore the potential ability of the upcoming Large Synoptic Survey Telescope (LSST Science Collaboration et al. 2009) to discover exoplanets via the transit method. We are specifically interested in the possibility of using LSST to search for exoplanets among distant stellar populations and late-type stars. Since the LSST project was not designed for the purposes of transit detection, there are a number of difficulties involved. The two most prominent are:

1. The magnitude range of stars observed by the LSST is too faint for candidates to be confirmed as exoplanets through standard observational methods, making it difficult to separate real exoplanets from the many type of false positives.
2. The cadence of LSST observations is much lower than current transit surveys, making correct extraction of transit-like events against background random noise more difficult.

On the other hand, these data will be delivered by LSST in large quantity, and it is prudent to examine just what kinds of exoplanets can be identified using this information. Even if specific exoplanets cannot be confirmed, it may be possible to statistically examine the set of candidates found, and derive bulk properties for the exoplanet population observed by LSST.

This paper is the first in a series that will model the predicted properties of the LSST data set. In that series, we will examine:

- What tools can be used to extract exoplanet transit candidates from the LSST light curves?
- What will be the dominant type of false positives?
- How can these false positives be mitigated, using either the LSST data itself or follow-up observations?
- What new populations of stars can be probed for planets with LSST that have not yet been searched as thoroughly?
- What do we predict will be the number and parameter distribution of exoplanets detectable with the LSST?

This sort of inquiry has been partially addressed by other papers. In the LSST Science Book (LSST Science Collaboration et al. 2009), Section 8.11 examines how many total transiting planets might be detected by LSST. Beatty & Gaudi (2008) also examined the bulk yield of transiting planets from LSST. We intend to build on these initial examinations by utilizing detailed LSST cadence and photometric performance applied to different types of stars, as well as incorporating updated information about the intrinsic frequency

of different planets sizes and periods from the *Kepler* mission in a future paper. In later papers will also seek to include realistic models of stellar binarity and variability, as well as other false positive sources, and investigate improvements to existing transit-detection algorithms customized for the LSST cadence and multiband data.

In this first paper, we present our statistical framework, and we demonstrate that certain types of interesting transiting planets should certainly be detectable in LSST data, even if they are not yet confirmable. We start by describing our method for modeling LSST light curves (§2). We then describe simple models for simulating transiting exoplanets in the light curves (§3), and computationally recovering the signals. We demonstrate that a number of scientifically interesting planet/star configurations should be readily detectable in LSST data, even with the use of standard transit-search routines (§4). Finally, we summarize our findings and describe the key challenges in this project.

2. Assumed LSST Parameters

The Large Synoptic Survey Telescope is an 8.4-meter telescope being constructed in Cerro Pachon, Chile, with first light planned in 2020 (Ivezic et al. 2008). LSST will survey approximately 30,000 square degrees of the sky repeatedly over the course of 10 years. Observation of a field will consist of two consecutive exposures of 15 seconds each, hereafter referred to as ‘visits’. For the majority of the sky, each field will have ~ 1000 visits. This will result in approximately 1 billion light curves that are sparsely-sampled over time. LSST will also have a few selected fields that will be observed at a much higher frequency, referred to as deep-drilling fields. Each of these fields will represent 1% of the total number of LSST observations and will receive $\sim 10,000$ visits over LSST’s scheduled operation. For both cadences (regular cadence and deep-drilling), these observations will be distributed among 6 different wavelength bands, *ugrizy*. LSST’s sensitivity will cover a magnitude range from $m \sim 16$ down to $m \sim 25$. In this section we describe the cadence and noise parameters that we adopt in our simulated light curves.

2.1. Cadence Model

To aid in the planning and evaluation of the science goals of LSST, the LSST team has developed the LSST Operations Simulator (OPSIM). This software tool includes models of the hardware and software performance, modeled site conditions, and an algorithm that determines which fields are observed each night, producing a list of observations with field ID, band, limiting magnitude, and numerous other parameters. The OPSIM represents a reasonable model of ten years of observations with LSST over the entire region of sky that will be observed, including both the regular and deep-drilling fields, while taking into account limiting factors such as weather, maintenance, and other physical constraints. For the purposes of this work we use the OPSIM v2.3.2, run 3.61 results¹ for two fields — one representative of a standard field, and one

¹Available at <https://www.lsstcorp.org/?q=opsim/home>

representative of a deep-drilling field — in order to focus on how often a given star would be observed based on a sample of the LSST cadence.

In Figure 1, we show the time between the beginning of exposures for both fields. In both cases, we have excluded nine intervals that represent the gaps between seasons of observing, and are on the order of 200 days. For the deep drilling field, it is worth noting that observing schedules focus on hour-long blocks of constant observation, and this constant observation results in a large peak at ~ 35 seconds, as this would allow for the exposure time plus the readout time and represents the minimum interval between most observations.

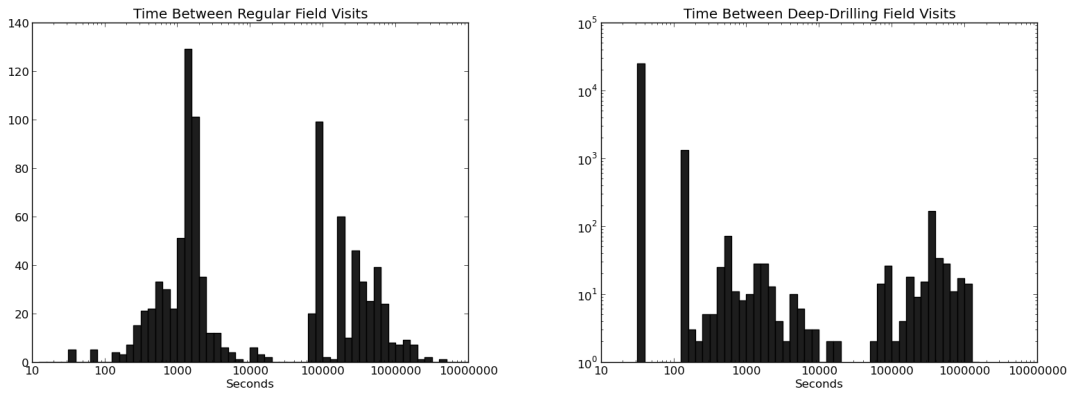


Fig. 1.— Time between beginning of exposures for a given field, with a regular cadence field displayed on the left. On the right, the deep-drilling field has a large portion of consecutive observations, resulting in a very significant portion of the results being at the time it will take for LSST to observe and read out the data.

2.2. Noise Model

The photometric noise in simulated LSST light curve comprises two components, a systematic noise floor and random photon noise. LSST’s systems are designed to maintain low systematic error, $\sigma_{sys} < 0.005$ mag. For purposes of this paper, the systematic error is treated conservatively as $\sigma_{sys} = 0.005$ mag. The random photon noise, dependent on the band being used, varies with changes in atmospheric extinction, stellar magnitude, and seeing conditions. Ivezić et al. (2008) define the random photometric error with the following equation:

$$\sigma_{rand}^2 = (0.04 - \gamma)x + \gamma x^2 \quad [\text{mag}^2] \quad (1)$$

In this equation, γ is a band-specific parameter, and $x = 10^{(m-m_5)}$. Here, m is the band-specific apparent magnitude and m_5 is the 5σ limiting magnitude for point sources. The quantity m_5 includes both band-specific parameters and factors such as seeing conditions, air mass, and exposure time. We can then express the total noise for a single visit:

$$\sigma^2 = \sigma_{sys}^2 + \sigma_{rand}^2 \quad (2)$$

In Figure 2, we look at the total noise for a single LSST visit to any field at the zenith. Here, we use the values Ivezić et al. (2008) provide for m_5 and γ . As transits of exoplanets frequently have depths on the order of 0.01 mag, Figure 2 shows that for apparent magnitude ~ 16 down to as far as ~ 20 for some bands the photometric noise is less than the depth that would be expected of a transit event. This represents a much fainter magnitude range with this level of photometric precision than most previous transiting planet searches have explored.

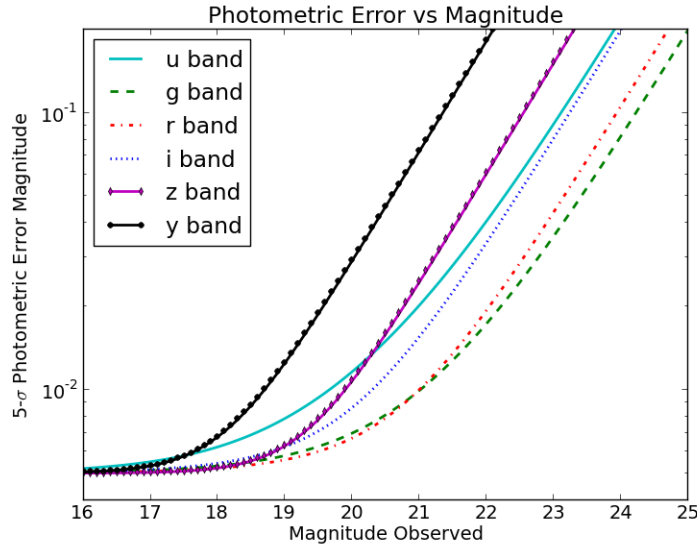


Fig. 2.— Noise model at zenith for LSST as a function of stellar magnitude in all observed bands. From Ivezić et al. (2008)

3. Simulated LSST Light Curves of Transits

3.1. Light Curve Construction

In order to characterize the ability of LSST to detect exoplanets, we create synthetic light curves to analyze the possibilities for detection of transit signatures. In §4 we define several star/planet configurations for simulated light curves, specifying for each the stellar mass, planetary radius, orbital period, and distance from Earth. Masses are converted to spectral types by interpolating the relations from Cox (2000). Based on spectral type, we obtain absolute magnitudes in the *ugriz* bands from Covey et al. (2007). While there is still much uncertainty about the specific parameters of the y-band filter that LSST will eventually use, for this work we use a y-band defined by Hodgkin et al. (2009).

Light curve generation itself requires orbital period, as well as transit depth and duration as determined by the geometry of the system, and the apparent magnitude of the host star in all bands. *Kepler* has shown

that while stars do have a wide range of intrinsic stellar variability, most will have variability of less than 1% (Basri et al. 2011). This intrinsic noise will be smaller than both the noise present in the observations and the transit depths we focus on, so we do not include that effect in these light curves. Transits are modeled as boxcars and when applied to the apparent magnitude of the star, allows us to create a noiseless lightcurve of the star that features the transit. We then add the photometric noise to the light curve, modeled as Gaussian noise, and dependent on apparent magnitude and band (See Figure 2) to create light curves similar to what LSST will observe.

The resulting light curve can be represented in all six bands. However, the transit depth will be independent of wavelength. Therefore we can median subtract the baseline of each light curve and combine them to create one unified light curve for enhanced transit detection. An example of a six-band light curve is shown in Figure 3. It is already noticeable in this case that the *u*-band will have the largest noise for the stellar populations in which we are most interested.

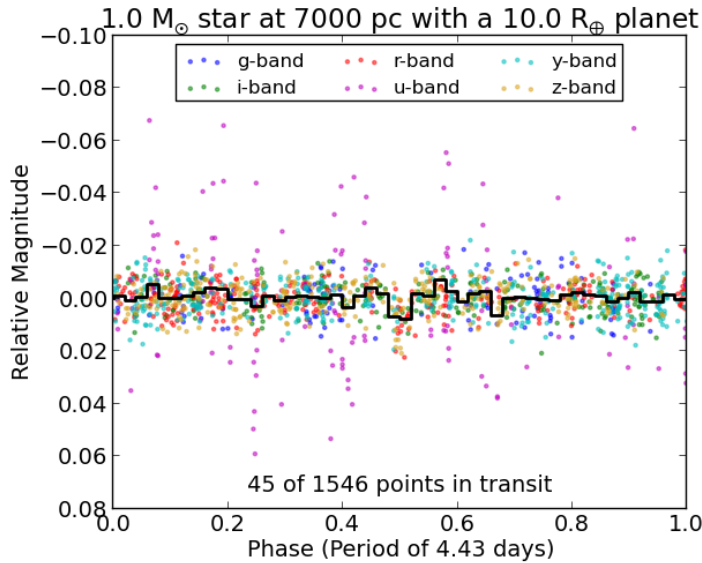


Fig. 3.— A sample six-band light curve, demonstrating the ability to combine all bands into a single phased light curve. The black line shows the binned data for the light curve.

The multiband nature of the observations will also provide additional information to characterize the light curves. Since exoplanet transits would be expected to be the same depth in all wavelengths, signals from eclipsing binary stars can be eliminated as planet candidates if we observe transit depths that are dependent on wavelength. Our intention in this paper is not to provide a rigorously developed number for expected exoplanet detections, or to address distinguishing planetary transits from other signals, but rather to demonstrate that exoplanets will be theoretically detectable, such that this is a worthwhile consideration as the LSST project moves forward.

3.2. Period Recovery

We demonstrate that transits can be recovered by searching for periodicity using the Box-fitting Least Squares (BLS) algorithm (Kovacs et al. 2002)². The BLS algorithm has been shown to be extremely powerful for detecting transits in high cadence data sets (Enoch et al. 2012). While LSST will not be a high cadence survey, we use this algorithm as an initial test of LSSTs capability for recovering transit signals. In order to examine the significance of these detections, we also measure the likelihood of having a peak of equal strength in the BLS periodogram by random chance, or due to some feature of the cadence, to measure a false alarm probability (FAP). To carry out this check, for each light curve we randomly rearrange the magnitude and time information, and then reapply BLS. We conduct that operation 1000 times for each light curve, and record the highest BLS peak in each case. The resulting data sets allows us to specify the 1% and 0.1% false alarm probabilities for BLS.

4. Results: Examples of Simulated Light Curves for Different Types of Transits

We begin examining detectability by creating simulated light curves (§3) to examine what exoplanet transits will look like for several different cases with stellar parameters outlined in Table 1. These are intended to exemplify well-studied populations of exoplanets as well as some populations that could prove very interesting but have not been a focus of planet searches thus far.

Table 1: Stellar Properties

Scenario		Band					
		m_u	m_g	m_r	m_i	m_z	m_y
G-dwarf at 7000 pc	Apparent Magnitude	21.433	20.066	18.699	18.540	18.500	17.913
	Standard Deviation	0.023	0.007	0.006	0.006	0.006	0.007
K-dwarf at 2000 pc	Apparent Magnitude	23.619	21.091	18.526	17.980	17.675	17.265
	Standard Deviation	0.149	0.011	0.005	0.005	0.005	0.006
M-dwarf at 400 pc	Apparent Magnitude	24.424	21.466	18.530	17.150	16.428	15.704
	Standard Deviation	0.286	0.013	0.005	0.005	0.005	0.005
G-dwarf at 50 kpc	Apparent Magnitude	25.658	24.334	22.968	22.807	22.770	22.183
	Standard Deviation	1.029	0.109	0.043	0.068	0.122	0.214

Table 1 calculates absolute magnitudes for *ugriz* bands from Covey et al. (2007) and *y* band from Hodgkin et al. (2009).

²We use the implementation of the BLS algorithm that is part of the VARTOOLS package(Hartman et al. 2008)

4.1. A Hot Jupiter Orbiting a G-dwarf in the Milky Way

The category of transiting exoplanets that have been studied most extensively are the Hot Jupiters, Jovian-mass planets orbiting sun-like stars with periods on the order of days. Here, we simulate a light curve for a $10.0 R_{\oplus}$ planet orbiting at 4.43 days around a $1.0 M_{\odot}$ star. The distance we have set the star at is 7000 pc from the Earth; this distance has been chosen so that the apparent magnitude of the host star is within the sensitivity range of LSST in all bands, while also representing a distance inaccessible to most current exoplanet surveys. Our resultant light curve is then phase folded on the input period in order to generate the phased light curve displayed in Figure 4. In this case, there is a very noticeable drop in the star’s brightness of 0.009 mag, showing that LSST can at least detect such a transit strong enough in the six-band lightcurve to be visually identifiable.

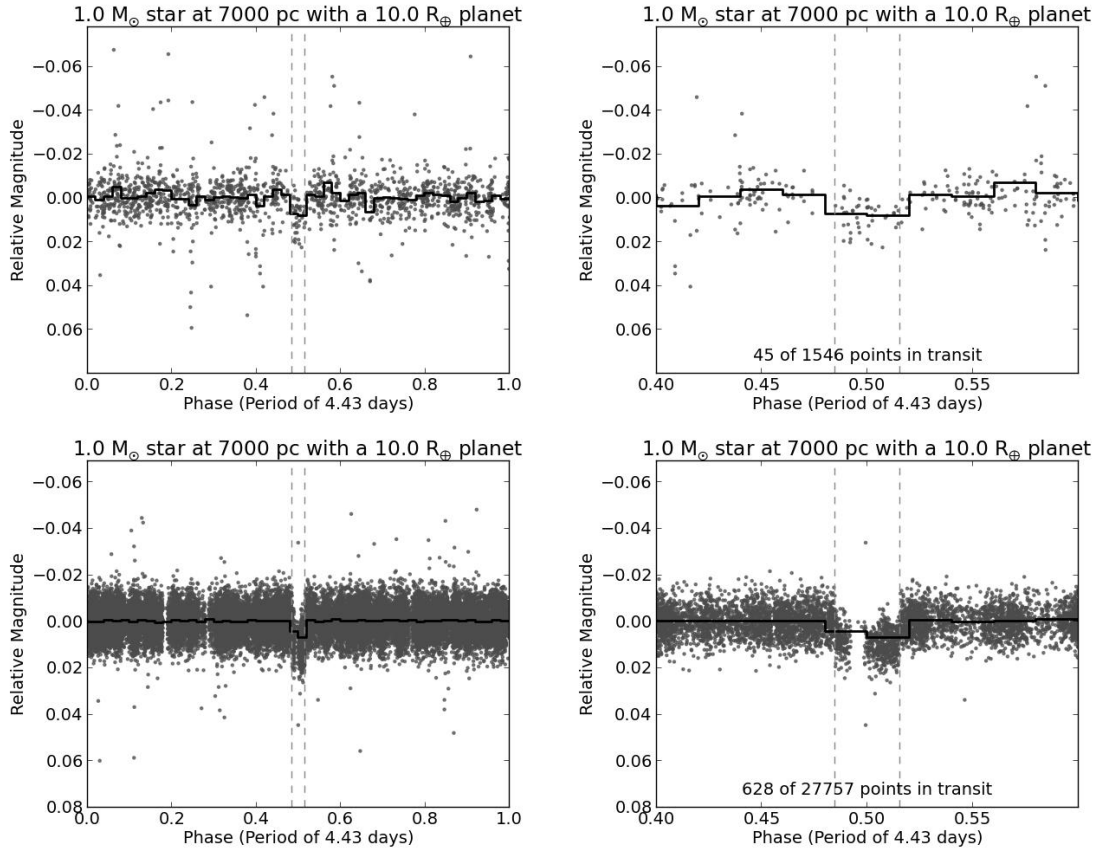


Fig. 4.— Light curve for a $10.0 R_{\oplus}$ planet in a 4.43 day period around a $1.0 M_{\odot}$ star at 7000 pc. The top two plots show a regular LSST field and the bottom two plots show an LSST deep-drilling field. The plots on the left show the full phase of the planet, and the plots on the right show the transit in particular. Black lines are binned data of the light curve.

For the Hot Jupiter case, we provide the BLS periodograms for both a regular LSST field and a deep-

drilling field in Figure 5. We also mark the true period on the periodogram, as well as the aliases at half and double the period. In both cases, the 4.43 day period is the highest peak in the periodogram, providing a qualitative reassurance that the periods visible in Figure 4 could be recovered had the value not been known. When we look at the likelihood at having a peak as high as the 4.43 day peak in our reordered light curves, we find that in 1000 light curves there are no peaks of equal or greater height, and from that we project the false positive rates for Hot Jupiters at both cadences as $<0.1\%$.

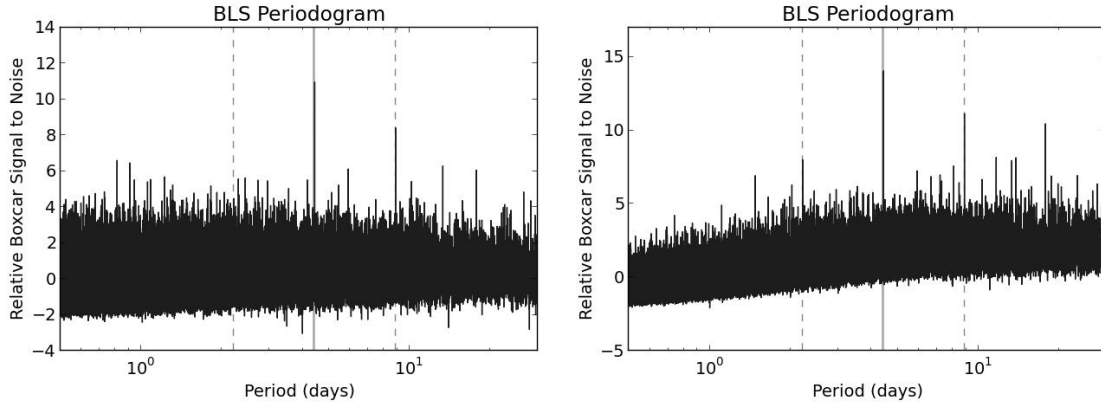


Fig. 5.— BLS periodogram for a Hot Jupiter in a standard field on the left, and a deep drilling field on the right. The lighter grey line marks the actual period of 4.43 days, while the other two dashed lines mark 2.215 and 8.86 days.

4.2. A Hot Neptune Orbiting a K-dwarf in the Milky Way

In our second case, we examine a Hot Neptune. Representing a regime between very large Jovian planets and smaller terrestrial planets, the Hot Neptune range has been richly populated by *Kepler* observations and represents planets with radii between 3 and 4 R_{\oplus} . Here we place a 4.0 R_{\oplus} planet in a 7.3 day period around a 0.6 M_{\odot} star at 2000 pc. Ground-based observations are generally limited in sensitivity of transits that are on the order of 1%, and so we have used a slightly smaller host star such that a Neptune-sized planet will still represent an approximately similar drop in brightness from the Hot Jupiter case. We have also moved the distance to the star to a closer location to maintain our constraint that the star’s apparent magnitude in all bands will be within the sensitivity range of LSST. As the transit events that we are examining will generally range somewhere between 3 mmag and 10 mmag in depth, we chose only to plot bands where the standard deviation is less than 30 mmag. In this light curve the noise in the *u*-band dominates the transit signal, and we only plot *grizy* bands. The transit in Figure 6 is not as visible as in the case of a Hot Jupiter, but can be discerned in the deep-drilling field where there are enough observations for the transit to be seen despite the noise.

In the Hot Neptune case, we provide the BLS periodograms for both a regular LSST field and a deep-

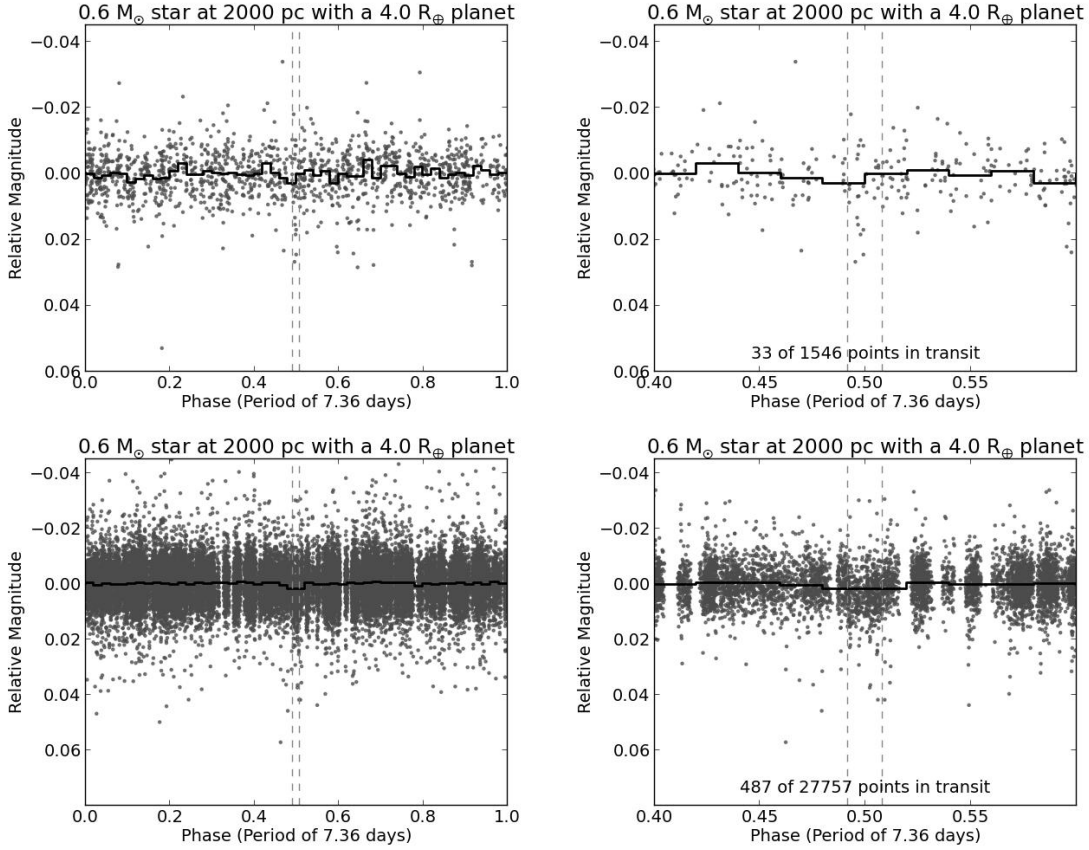


Fig. 6.— A $4.0 R_{\oplus}$ planet in a 7.36 day period around a $0.6 M_{\odot}$ star at 2000 pc. The top two plots show a regular LSST field and the bottom two plots show an LSST deep-drilling field. The plots on the left show the full phase of the planet, and the plots on the right show the transit in particular. Black lines are binned data of the light curve.

drilling field in Figure 7, and indicate the true period and two aliases of it. For the regular LSST field BLS does not recover the period and there are no strong discernable features in the periodogram that would correspond to the planet period. However, BLS does recover the input period for the deep-drilling field. This peak is higher than all but one BLS period from our 1000 permuted light curves, and we calculate a false positive rate of 0.1%.

4.3. A Super-Earth Around an M-dwarf in the Milky Way

For our final Milky Way case, we pick a $2.0 R_{\oplus}$ planet in a 5.37 day period around a $0.3 M_{\odot}$ star at 400 pc. The choice of this case is twofold; red dwarfs have not been frequently targeted in planet searches and a Super-Earth around a red dwarf will still be a significant enough transit depth to warrant some consideration

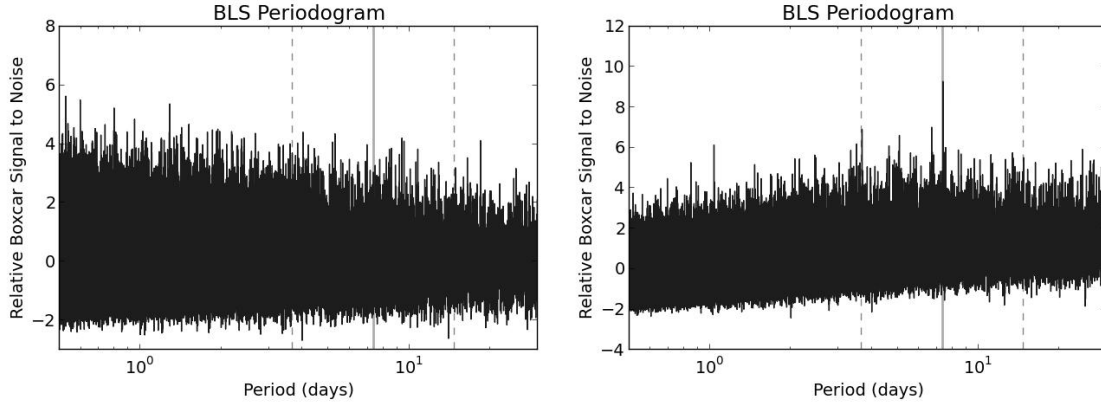


Fig. 7.— BLS periodogram for a Hot Neptune in a standard field on the left, and a deep drilling field on the right. The lighter grey line marks the actual period of 7.36 days, while the two dashed lines mark 3.68 and 14.72 days.

for ground-based observations. The distance has again been adjusted so that the apparent magnitude of the red dwarf is approximately still within LSST’s sensitivity range. As in the previous case, the u -band is omitted. While in the standard field the transit is not visually detectable in Figure 8, in the deep-drilling field a small but slightly noticeable transit event is visible in the 5 remaining bands. With what appears to be a detectable signal in the deep-drilling field, we further explore a red dwarf host star with a Super-Earth in a larger period, moving the planet out to a period of 24.37 days. Our motivation in choosing this period is that for a red dwarf of this mass, a planet in a ~ 25 day period will be in the habitable zone, and this planet’s system environment would be similar to that calculated for some planets in the Gliese 667C system (Gregory 2012). While this decreases the number of points in transit, the transit shown in Figure 9 appears to still be visually detectable for a deep-drilling field.

For both the 5.37 and 24.37 day periods, and at both cadences, BLS doesn’t recover the input period or an alias as the top peak. It is notable, however, that for the 24.37 day period in a deep-drilling field, the input period is the second highest peak that BLS recovered. By looking at the top two peaks from BLS for 1000 permutations of the simulated habitable Super-Earth light curve in a deep-drilling field, we find that there are 390 higher peaks, which we translate to a false positive rate of 19.5%. Looking at the periodograms in Figure 10 does show, however, that there is still potentially useful information present in the BLS results. While there appears to be no compelling features in the two lefthand figures that represent the two periods in regular fields, there are notable features in the deep-drilling fields on the right. For the 5.37 day period, the two highest peaks are the initial period and half the period. Similarly, for the 24.37 day period the initial period is one of the highest peaks, and there is a notable peak at half the period as well. While these period recoveries lack the rigor of being the top peak recovered by BLS, this does provide an indication that the transits could still be more reliably recovered in deep-drilling fields with the application of additional methods.

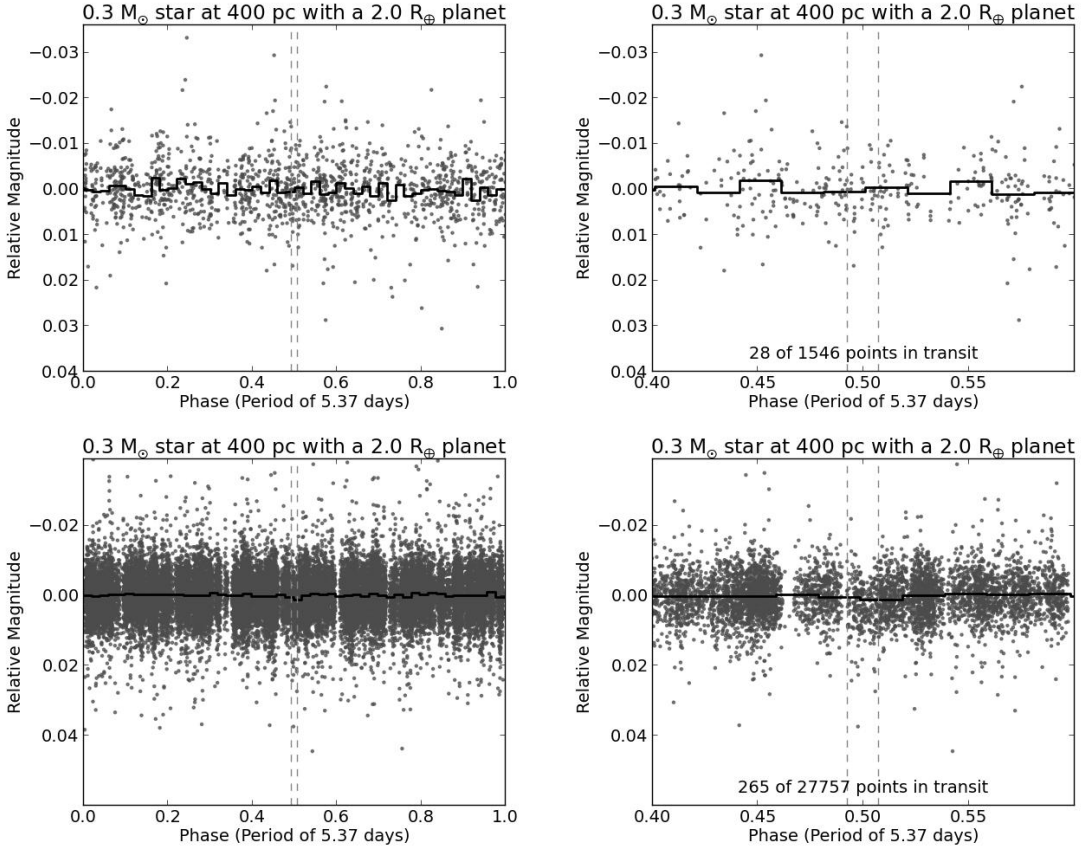


Fig. 8.— A $2.0 R_{\oplus}$ planet in a 5.37 day period around a $0.3 M_{\odot}$ star at 400 pc. The top two plots show a regular LSST field and the bottom two plots show an LSST deep-drilling field. The plots on the left show the full phase of the planet, and the plots on the right show the transit in particular. Black lines are binned data of the light curve.

4.4. A Hot Jupiter in the Large Magellanic Cloud

LSST will also provide a unique opportunity to look for exoplanets outside of the Milky Way. Fields that have been proposed for LSST to observe at higher cadence include the Large Magellanic Cloud (Szkody et al. 2011), and based on the faintness that LSST will be capable of, we also demonstrate that LSST should have the potential to be sensitive to Hot Jupiters transiting stars located in the Large Magellanic Cloud. For this example, we look at a slightly larger Hot Jupiter than before, here a $13 R_{\oplus}$ planet with a 4.4 day period orbiting a $1.0 M_{\odot}$ star at 50,000 parsecs from Earth in Figure 11. As in the previous two examples, the u -band data has been omitted, but at this faintness the noise is sufficiently large that we also ignore gzy -bands and only plot the ri -bands. While the LSST fields do not seem to have any visible sign of a transit, BLS does have greater success, as shown in Figure 12.

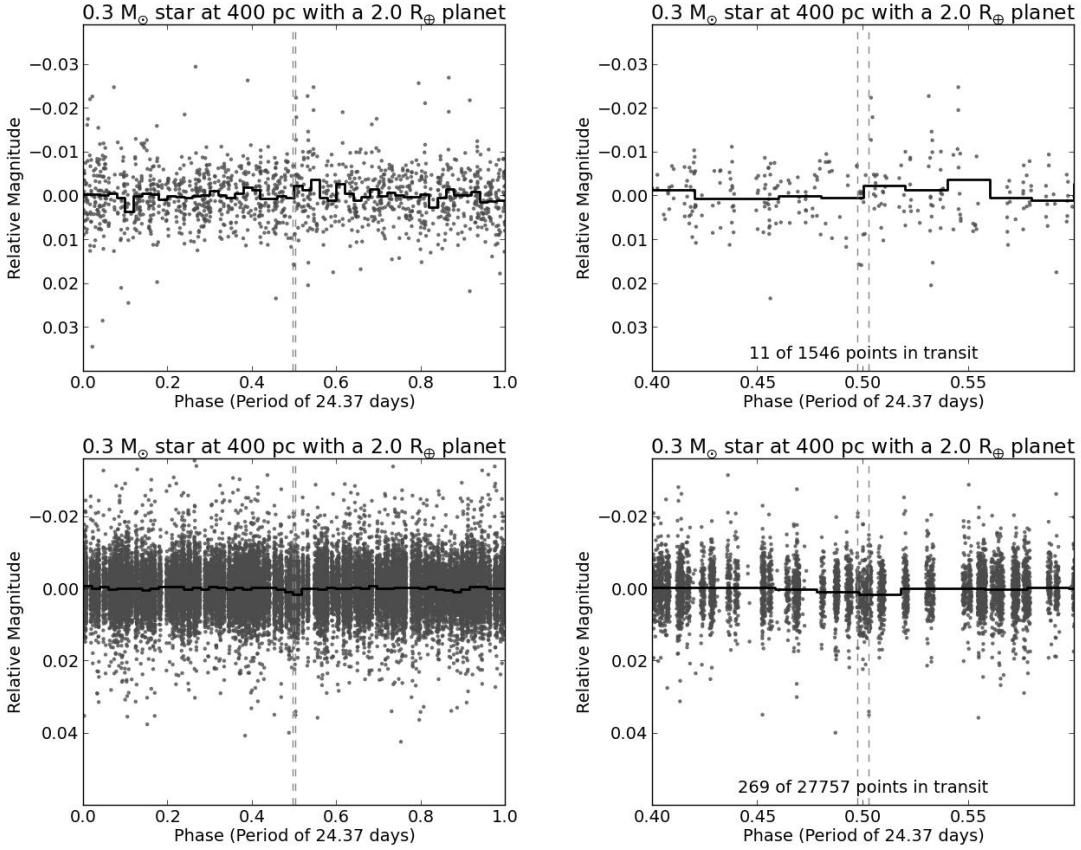


Fig. 9.— A $2.0 R_{\oplus}$ planet in a 24.37 day period around a $0.3 M_{\odot}$ star at 400 pc. The top two plots show a regular LSST field and the bottom two plots show an LSST deep-drilling field. The plots on the left show the full phase of the planet, and the plots on the right show the transit in particular. Black lines are binned data of the light curve.

The entire set of deep-drilling fields has yet to be chosen, although the first four deep-drilling fields to be selected from LSST white papers have been intended for observations of distant galaxies (Gawiser et al. 2011; Ferguson 2011). However, other deep-drilling fields have also been suggested with the intention of focusing on the Large and Small Magellanic Clouds (Szkody et al. 2011). These fields for the LMC and SMC would have an observing schedule which limits the filters used, and is proposed to only use *gr* band observations. This would be consistent with the limitations on photometric precision in our final light curves, which do not include several bands that we omitted due to high noise, and may result in light curves with much better photometric precision.

For a Hot Jupiter in the Large Magellanic Cloud, we provide the BLS periodograms for both a regular LSST field and a deep-drilling field in Figure 12, and indicate the true period and two aliases of it. BLS does not recover the period in a regular field, nor do there seem to be any notable features in the periodogram,

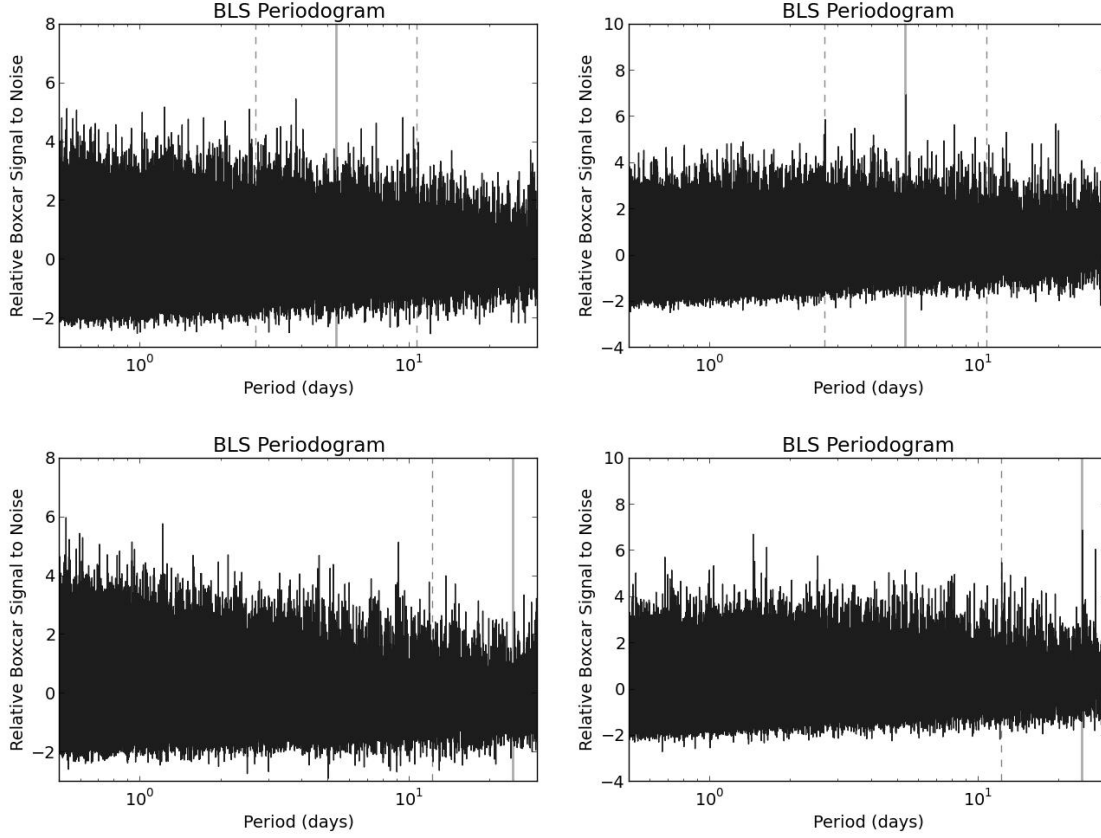


Fig. 10.— BLS periodograms for a Super-Earth in a regular field on the top and in a deep-drilling field on the bottom. The 5.37-day period is on the left and the 24.37-day period is the right. The lighter grey line marks the actual period for each scenario.

however we do recover the period in the deep-drilling field with a peak height that indicates a false positive rate of less than 0.1%. This result demonstrates that LSST could conceivably detect a planet candidate outside the Milky Way. While it is worth noting that at the distance of the LMC it would be very difficult to confirm an exoplanetary candidate, this would certainly be a novel discovery and give some broader indication of planet formation processes in other environments.

5. Discussion

We have demonstrated that using already developed algorithms, LSST will have the sensitivity to detect exoplanet transits for an array of exoplanets and host stars, and at varying distances. These results are summarized in Table 2. However, these capabilities will be greatly shaped by the selection process for the remaining deep drilling fields, as the selection of the LMC or SMC for deep drilling will greatly increase

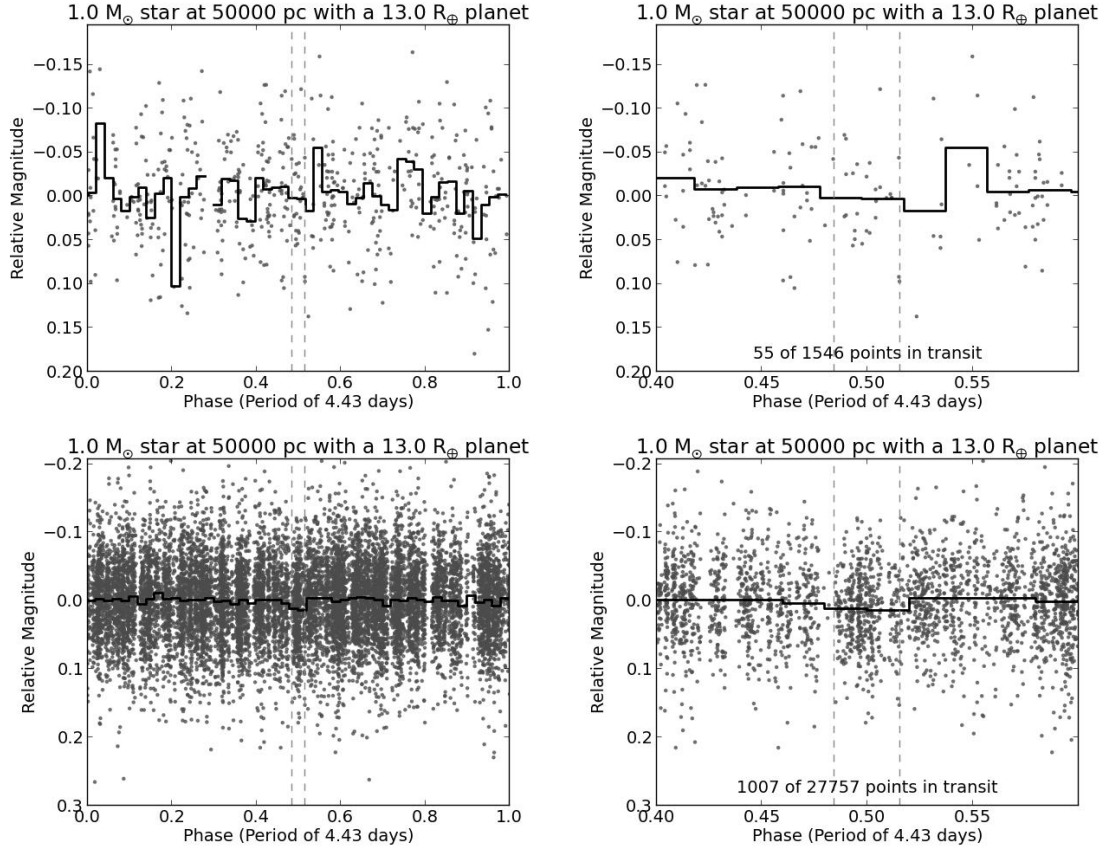


Fig. 11.— A $13.0 R_{\oplus}$ planet in a 4.43 day period around a $1.0 M_{\odot}$ star at 50,000 pc. The top two plots show a regular LSST field and the bottom two plots show an LSST deep-drilling field. The plots on the left show the full phase of the planet, and the plots on the right show the transit in particular. Black lines are binned data of the light curve.

the ability to get visually identifiable transits in those light curves.

For the case of Hot Jupiters, specifically, we can make a very preliminary approximation of the number of planets that could be recovered by LSST. Restricting our focus to the g -band, we find the number of stars between 16th and 22nd magnitude in a one-square-degree field at around 1800 stars, according to TRILEGAL 1.6³. There will, additionally, be around 30,000 square degrees observed, for a total of 54 million stars observed. Of these, we would expect around 0.5% of dwarf stars to host Hot Jupiters, and the likelihood of a Hot Jupiter to transit its host star is $\sim 10\%$. This would result in 27000 transiting Hot Jupiters, and recovering just 5% of these Hot Jupiters would result in over 1000 new Hot Jupiters discovered. While these are very approximate numbers, they do indicate the large potential that LSST possesses.

³Available at <http://stev.oapd.inaf.it/cgi-bin/trilegal>

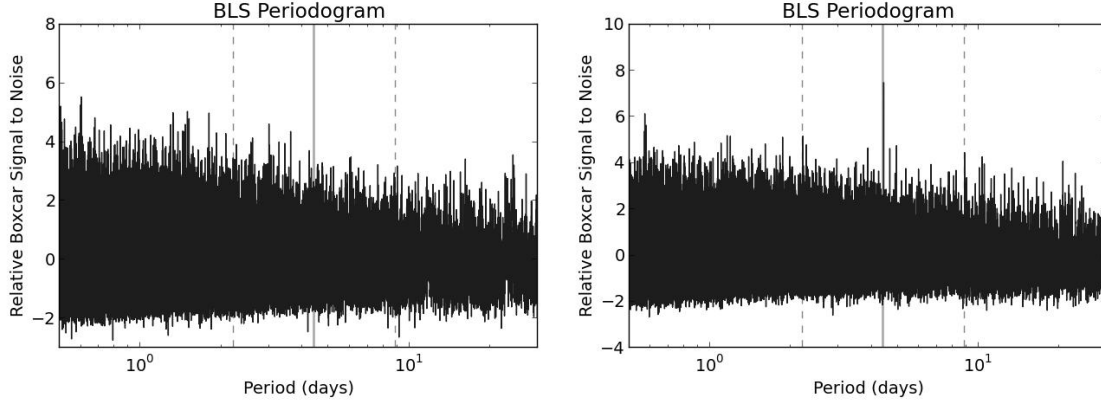


Fig. 12.— BLS periodogram for a Hot Jupiter orbiting a star in the LMC in a regular field on the left and a deep-drilling field on the right. The lighter grey line marks the actual period.

Table 2: Scenario Detection

Cadence	Scenario				
	G-dwarf at 7000 pc Hot Jupiter	K-dwarf at 2000 pc Hot Neptune	M-dwarf at 400 pc Super-Earth (4.4 d)	M-dwarf at 400 pc Super-Earth (25.3 d)	G-dwarf at 50 kpc Hot Jupiter
Standard	Yes	No	No	No	No
False Positive Percent	<0.1	–	–	–	–
Deep-Drilling	Yes	Yes	No	No	Yes
False Positive Percent	<0.1	0.1	–	–	<0.1

Table 2 lists whether or not the best period from VARTOOLS BLS algorithm is consistent with the input period for each of the scenarios described in §4 (and listed at the top of each column). The rows represent a standard cadence field and a deep-drilling field. Also included is the false positive rate when the period was correctly recovered by BLS.

Through our work thus far, we have treated host stars as having no intrinsic variability, however a more sophisticated model of stellar light curves will be needed going forward. Stellar variation from rotation, pulsating, flaring, and eclipses will need to be included to better synthesize the kinds of light curves that will likely be observed by LSST, as these variations will complicate recovering the variation caused by a transiting planet and be a source of false negatives. Additionally, these variations will also need to be incorporated in order to properly create the false positives that will also exist in LSST fields.

A greater difficulty will be developing methods that can more rigorously detect and recover these transits, and determine the difference between likely exoplanetary candidates and false positives, astrophysical or otherwise. Due to the low cadence of the data, standard methods used for finding periodic signals in light curves are potentially not sufficient to find transits in all circumstances, and newer algorithms will need to be implemented with these constraints in mind. The efficiency of these algorithms will be an important question, both to quantify the usefulness that LSST will have in detecting extrasolar planets, and in determining

the best way to structure a search for transiting planets in the LSST data once observations begin in 2020.

There will also be a need to expand this study from the discrete examples we have set forth here, and apply similar analysis to a more diverse set of systems. That will include expanding our synthetic light curves to represent a distribution of stellar masses and exoplanet radii and periods, as well as factoring in the likelihood that a planet will transit. This will allow our results to look not just at the likelihood for a given planet to be detected, but rather to determine how many exoplanets could reasonably be detected among stellar populations such as field stars and star clusters. Furthermore, we hope to characterize these planets to look at what sorts of planets will be easiest to detect using the LSST data.

While we have primarily discussed potential opportunities for exoplanet detection from LSST observations specifically, these same methods can be applied to other surveys that have a large number of observations over relatively long baselines, but with similarly sparsely-sampled data that will make extracting exoplanetary transits difficult without implementing more novel algorithms. Surveys that would warrant such consideration may include Pan-STARRS (Kaiser 2004), the Catalina Real-Time Sky Survey (Djorgovski et al. 2011), the Palomar Transient Factory (Rau et al. 2009), and GAIA (Jordi & Carrasco 2006). Once our procedures for stellar and exoplanetary population simulation, light curve creation, and application of detection algorithms have been developed for LSST, we will then be able to apply these same techniques to these other surveys to greatly increase the data available to search for exoplanets in varied situations.

REFERENCES

- Bakos, G., & Hartman, J. 2011, EPJ Web of ..., 1, arXiv:1101.0322v1
- Basri, G. et al. 2011, AJ, 141, 20
- Batalha, N. M. et al. 2013, ApJS, 204, 24, arXiv:1202.5852
- Beatty, T. G., & Gaudi, B. S. 2008, ApJ, 686, 1302
- Covey, K. R. et al. 2007, AJ, 134, 2398
- Cox, A. N. 2000, Allen’s Astrophysical Quantities, Vol. 53, 719
- Djorgovski, S. G. et al. 2011, 6, arXiv:1102.5004
- Doyle, a. P. et al. 2012, MNRAS, 428, 3164
- Enoch, B., Haswell, C. A., Norton, A. J., Collier-Cameron, A., West, R. G., Smith, A. M. S., & Parley, N. R. 2012, Astronomy & Astrophysics, 548, A48
- Ferguson, H. 2011, lsstcorp.org, 1
- Fischer, D. a., Marcy, G. W., & Spronck, J. F. P. 2014, ApJS, 210, 5
- Gawiser, E., Newman, J., Zhan, H., & Ballantyne, D. 2011, lsstweb.lsstcorp.org, 1

- Gregory, P. C. 2012, 16, arXiv:1212.4058
- Hartman, J. D., Gaudi, B. S., Holman, M. J., McLeod, B. A., Stanek, K. Z., Barranco, J. A., Pinsonneault, M. H., & Kalirai, J. S. 2008, ApJ, 675, 1254
- Hodgkin, S. T., Irwin, M. J., Hewett, P. C., & Warren, S. J. 2009, MNRAS, 394, 675, arXiv:0812.3081v3
- Howard, A. W. et al. 2012, ApJS, 201, 15
- Ivezic, Z. et al. 2008, 34, arXiv:0805.2366
- Jordi, C., & Carrasco, J. 2006, PASP, 364, 215
- Kaiser, N. 2004, in Proc. SPIE, ed. J. M. Oschmann, Jr., Vol. 5489, 11–22
- Kovacs, G., Zucker, S., & Mazeh, T. 2002, A&A, 391, 369
- LSST Science Collaboration et al. 2009, LSST Science Book, version 2. edn. (Tucson, AZ: LSST Science Collaboration), 596
- O’Donovan, F. T., & Charbonneau, D. 2007in , 6, arXiv:0705.1795
- Patel, S. G., Vogt, S. S., Marcy, G. W., Johnson, J. A., Fischer, D. A., Wright, J. T., & Butler, R. P. 2007, ApJ, 665, 744, arXiv:0704.3418v1
- Pepper, J. et al. 2007, PASP, 119, 923
- Petigura, E. a., Howard, A. W., & Marcy, G. W. 2013, Proceedings of the National Academy of Sciences of the United States of America, 2013, 1
- Poleski, R., McCullough, P. R., Valenti, J. a., Burke, C. J., Machalek, P., & Janes, K. 2010, ApJS, 189, 134
- Rau, A. et al. 2009, PASP, 121, 1334, arXiv:0906.5355v1
- Szkody, P., Long, K., CfA, R., & Henden, A. 2011, lsstcorp.org, 1
- Tinney, C. G., Butler, R. P., Marcy, G. W., Jones, H. R. A., Penny, A. J., Vogt, S. S., Apps, K., & Henry, G. W. 2001, ApJ, 551, 507
- Youdin, A. N. 2011, ApJ, 742, 38
- Zechmeister, M. et al. 2013, Astronomy & Astrophysics, 552, A78, arXiv:1211.7263v1